Available online at www.sciencedirect.com
ScienceDirect
Carbon 45 (2007) 636–648
CARBON
www.elsevier.com/locate/carbon

Nanodiamond nucleation below 2273 K at 15 GPa from carbons with different structural organizations

Corentin Le Guillou [a,*], Fabrice Brunet [a], Tetsuo Irifune [b], Hiroaki Ohfuji [b], Jean-Noël Rouzaud [a]

[a] *Laboratoire de Géologie, CNRS UMR8538, 24 rue Lhomond F-75231 Paris cedex 05, France*
[b] *Geodynamics Research Center, Ehime University, 2-5 Bunkyo-cho, Matsuyama 790-8577, Japan*

Received 4 June 2006; accepted 5 October 2006
Available online 15 December 2006

Abstract

Five precursors covering the whole range of carbon structural organization, *i.e.* a quasi-amorphous soot (QAS), a raw carbon black (CB), a carbon black heat-treated at 2600 °C (HTCB), a polycrystalline graphite (PCG) and a highly oriented pyrolytic-graphite (HOPG) were run at 15 GPa in the 1500–1900 °C range between 15 and 60 min. Full transformation into nano-diamonds was not always achieved and the corresponding run products preserved the tracks of the transformation mechanisms which led to diamond formation. These mechanisms and their kinetics were characterized combining X-ray powder diffraction, Raman micro-spectroscopy and high-resolution TEM. Globally, the disordered precursors react faster than the crystalline ones: they achieve higher transformation rates and become transparent more easily. For the spherical CB particles, nano-diamond preferentially nucleates in their centre. The graphitic layers in the QAS directly transform into diamond without any prior graphitization. The crystalline organization is even found to decrease for the graphitized precursors (HTCB and PCG) as evidenced by HRTEM images showing graphite delamination. These precursors mostly evolve according to a diffusion-limited reconstructive mechanism which initiates at the precursor structural defects. HOPG behaves differently since it mostly transforms into lonsdaleite rather than cubic diamond.

1. Introduction

The graphite–diamond transition corresponds to a transformation from a highly anisotropic structure with two types of bonds (strong sp^2 bonds in the graphene layers and weak Van der Wals forces responsible for the layers stacking) to the hardest known material which is formed of purely covalent carbon-bonds (sp^3).

The activation energy of this transition is so great that diamond synthesis is a process that requires pressures (P) and temperatures (T) far above those of the diamond–graphite equilibrium boundary, unless catalyst materials are used. As a consequence, direct conversion (without catalysts) from graphite leads to diamonds of nanometre size.

It has been shown that the use of disordered carbon-forms (e.g. amorphous carbon, [1,2]) lowers the minimum P and T conditions of diamond synthesis. However, it remains unclear whether this higher kinetics of diamond formation is due to a lower activation energy of the disordered carbon–diamond transformation or if it is rather related to the higher level of metastability of disordered carbon (e.g. low density) compared to graphite (*i.e.* increase of the thermodynamic driving force to form diamond).

Accordingly, we have investigated the transformation mechanisms towards diamond of a variety of carbons which encompass a wide range of structural order. For example, we used, on one hand, perfectly crystalline

* Corresponding author. Fax: +33 144322200.
E-mail address: cleguill@clipper.ens (C.L. Guillou).

0008-6223/$ - see front matter © 2006 Elsevier Ltd. All rights reserved.
doi:10.1016/j.carbon.2006.10.005

graphite (HOPG, highly oriented polycrystalline graphite) and, on the other hand, carbon blacks and quasi-amorphous soots, which are composed of carbon nanoparticles with different microtextures and different levels of structural organization.

HOPG was chosen as a reference of defect-free (at the Raman scale) perfectly crystalline structure. In comparison, polycrystalline graphite has a smaller grain size and thus contains more defects, mainly concentrated at the crystallite boundaries, and leading to a significant Raman defect band. Carbon blacks and quasi-amorphous soot were chosen because they are assumed to contain numerous structural defects (sp^3 bonds instead of sp^2, pentagon cycles instead of hexagons). They are both strongly disordered but present totally different microtextures, as shown by HRTEM. The CB has a concentric microtexture (the nanometre sized polyaromatic structural units present an onion-like microtexture), whereas the very small graphene layers of the QAS are randomly distributed. Carbon blacks heated at 2600 °C at ambient pressure give partially graphitized concentric polyhedral nanoparticles. Their structural organization is equivalent to the polycrystalline graphite; but their crystallites (facets of the so-obtained polyhedra) show a concentric microtexture instead of a lamellar orientation in the polycrystalline graphite (see Fig. 3).

All starting materials were run less than 1 h in a multi-anvil press at 15 GPa in the 1500–1900 °C range. The run products were then characterized by using (1) X-ray powder diffraction (XRPD) in order to estimate the transformed volume fraction at the cubic millimetre scale, (2) high-resolution transmission electron microscopy (HRTEM) for a descriptive information about the structure and the microtexture of the run products at the nanometre scale and (3) quantitative Raman micro-spectroscopy to characterize the structural order (crystallite sizes, amount of defects, hetero-atoms, etc.) of the carbon products at the micrometre scale.

2. Experimental

2.1. HP-HT device

Experiments were performed at 15 GPa in a split-sphere multi-anvil apparatus (GRC, Matsuyama, Japan) using WC anvils with 5-mm truncation edge-lengths. The multi-anvil assembly (Fig. 1) is composed of a semi-sintered (Mg,Co)O octahedron filled with a straight-wall $LaCrO_3$ heater itself sandwiched between two ZrO_2 end-disks which are drilled to fit an axial molybdenum rod (electrical conductor). The junction of a $W_{97}Re_3$/$W_{75}Re_{25}$ thermocouple (0.125 mm diameter) is placed at mid-height of the $LaCrO_3$ heater, between the two sample containers (Pt capsules). Each sample fits in a NaCl sleeve to prevent contact with the furnace. NaCl ensures nearly hydrostatic pressure conditions around the samples. No chemical reaction between the NaCl sleeves and $LaCrO_3$ heater was observed. The temperatures and pressures will be given in the following with an uncertainty of 100 °C and 1 GPa, respectively.

The nominal oil-pressure is reached in 4 h, then samples are heated up to the nominal temperature (1500 °C, 1700 °C and 1900 °C) at an average rate of about 150 °C/min. Run durations are comprised between 15 and 60 min.

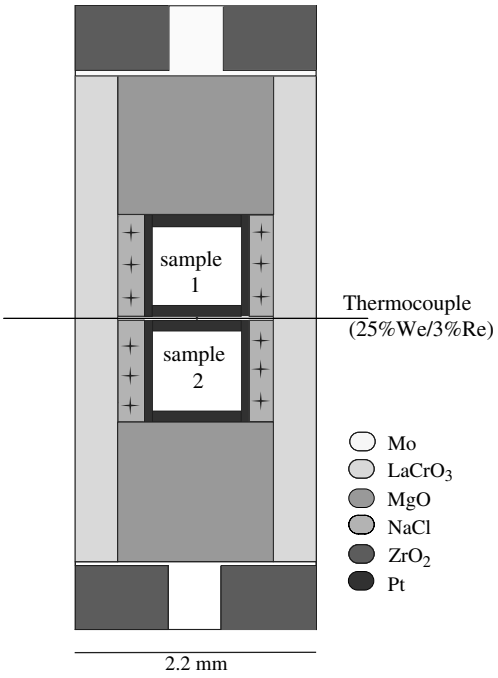

Fig. 1. High pressure cell with NaCl sleeves used for the multi-anvil experiments.

2.2. X-ray powder diffraction (XRPD)

Powdery samples were characterized using a MAC Science™ diffractometer (θ–2θ geometry) equipped with a rotating anode (Cu Kα) operated at 40 kV and 100 mA (graphite monochromator). However, most run products are sintered and contain significant amount of diamond; they cannot be crushed easily. The top of the platinum capsule in contact with the thermocouple junction is removed by polishing with sand paper to uncover the sample. Micro-diffraction is then possible and we used a MAC Science™ micro-focus diffractometer (50 μm X-ray beam) operated at 40 kV and 200 mA. The capsule is then set on a three circle goniometer. XRPD peak intensity cannot be directly used to compare diamond formation rates since the residual graphitic carbons display very different structural orders from one experiment to the other. In addition, even though the sample is rotated, textural effect is likely to influence basal reflection intensity. Owing to these complications, XRPD data are only used, in this study, to infer the presence or the absence of remaining graphitic material. However, optical inspection of the sample appeared to be a more sensitive tool to identify diamond-pure samples.

The mean diamond crystallite size was estimated using the Scherrer relation applied to the full width at half maximum (FWHM) of the 1 1 1 reflection $t = \frac{\lambda}{\Delta\theta * \cos\theta * K}$, where t is the mean crystallite thickness, λ the incident-beam wavelength, θ the diffraction angle, $\Delta\theta$ the FWHM, and K an experimental empirical factor which is usually taken equal to 0.9.

2.3. Raman microspectrometry

Raman spectra were mainly collected in the 500–3000 cm^{-1} range with a Raman microspectrometer (Renishaw Invia) using a 20 mW Argon laser (514.5 nm and 735 nm, Spectra Physics) and a LEICA (50×) magnification objective (0.5 numerical aperture). The UV Raman spectrum (244 nm) was collected with a Labram microspectrometer at the Ecole Normale Supérieure de Lyon.

For diamond, the first phonon mode corresponds to the stretching of sp^3 bonds and comes out at 1331 cm^{-1}. The first phonon mode

corresponding to sp^2 graphite stretching appears at 1580 cm^{-1} (G) for well crystallized products, while others bands at 1350 cm^{-1} (D1), 1620 cm^{-1} (D2) and sometimes around 1500 cm^{-1}, usually called defect bands, appear within disordered carbons [3]. Here, we used the area ratio $R = D1/(G+D1+D2)$ to quantify the relative degree of structural order in the studied materials [4].

2.4. High resolution transmission electron microscopy (HRTEM)

A JEOL 2010 microscope with an acceleration voltage of 200 kV has been used for this study. Very high magnification (400–800×) was necessary to observe the lattice fringe of both graphitic carbons ($d_{002} = 0.3354$ nm for graphite, >0.34 nm for the disordered carbons) and diamond ($d_{111} = 0.206$ nm).

Because of the extreme diamond hardness, it was difficult to prepare diamond rich samples by simple milling which causes strong contamination from the mortar. Consequently, thin (~0.1 μm) sections were prepared with the focused ion beam (FIB) technique. The thickness of the FIB section is generally about 150 nm. This is thin enough for electron transmission although not optimal since crystal superposition often occurs, deteriorates the image quality. The most interesting images are obtained when a diamond crystal lies on a 110 plane because then two 1 1 1 planes are under the Bragg conditions at the same time, and twinned crystals appear.

3. Results

3.1. Starting material characterization

Five different starting materials have been used: highly oriented polycrystalline graphite (HOPG), polycrystalline graphite (PCG), a carbon black (CB), the same carbon black but heat-treated at 2600 °C (HTCB) and a quasi-amorphous soot (QAS). They cover a wide range of structural organization with various microtextures at the nanometre scale which can respectively be compared in terms of transition mechanisms.

The *highly oriented polycrystalline graphite* (HOPG) has a perfect crystallographic structure (crystallites size of several microns) without any defects ($R \sim 0\%$, Fig. 2). It is synthesized from a pyrolytic carbon re-heated under pressure. It represents the end member of a highly crystalline structure.

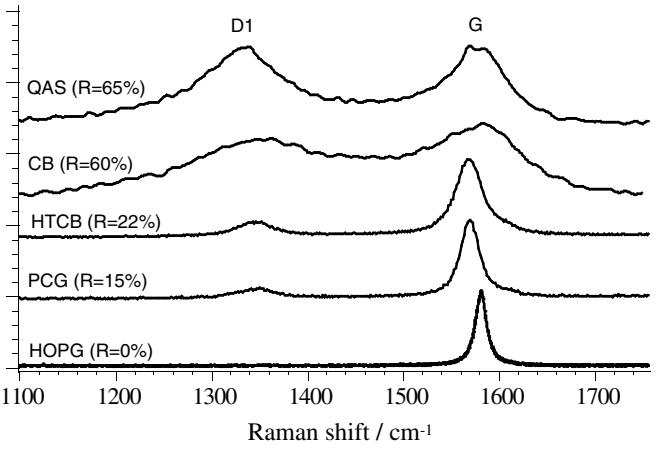

Fig. 2. First-order Raman spectra of the starting materials. The relative surface of the D1 bands is correlated to the structural order degree.

The *polycrystalline graphite* is composed of crystallites with typical sizes of 0.5–1 μm (Fig. 3a). This starting material has been used to obtain ultrahard nanodiamonds aggregates [5]. Since PCG crystallites are smaller than the laser beam spot, grain boundaries defects are also sampled by Raman micro-spectrometry. Consequently, compared to a micrometre large graphite single-crystal, PCG presents a D1 defect band, and a rather high R ratio, around 15% (Fig. 2).

The *carbon black* is a commercial PRINTEX 25 (Degussa) which is obtained by incomplete combustion of hydrocarbons. The particles are quasi-spherical with a diameter of 30–100 nm. Compared to PCG, this carbon black is a poorly ordered carbonaceous material made of small polyaromatic layers (about 1 nm average length), usually stacked by about 2 or 3 with a turbostratic order; the so-formed structural units exhibits a concentric microtexture (Fig. 3b). The centre is supposed to have a higher defect concentration, which are assumed to be pentagons, sp^3 bonds, ... The R ratio of this starting material is high (around 60%, Fig. 4) as expected for a strongly disordered carbonaceous material made of short polyaromatic layers.

The *HTCB* is obtained by heating the PRINTEX 25 at 2600 °C under an argon flow. This heat treatment does not increase the size of the particles [6]. The initially rounded nanoparticles are now polyhedral and partially graphitized (*i.e.* partial triperiodic order within the largest particles, Fig. 3c). The initial CB concentric microtexture has polygonized and each facet is now made of stacks graphitic layers. Actually, the R ratios of HTCB and PCG are also comparable, 22% and 15%, respectively (Fig. 2) and it is thus possible to test the specific influence of the concentric microtexture for a comparable amount of defects.

The *quasi-amorphous soot* (QAS) is the residue after toluene extraction of fullerenes from an electrical arc product. Raman shows a very low structural order for the QAS which is however not fully amorphous since the G and D bands remain distinct ($R \sim 65\%$). HRTEM images show short (about 1 nm), mostly unstacked, and randomly oriented (Fig. 3d) polyaromatic layers. Therefore, these nanoparticles are not *stricto sensu* amorphous. The numerous structural defects (as sp^3 or pentagons) limit the spatial extension of these layers, favour their curvature and prevent their stacking. This sample has to be compared with CB, because it has about the same amount of defects but shows no specific layers orientation.

3.2. X-ray powder diffraction of the HP and HT experimental products

The five starting materials described above were run at 15 GPa in the 1500–1900 °C range for durations comprised between 15 min and 1 h (Table 1).

At 15 GPa and 1500 °C, nano-diamonds are found to have crystallized from all starting materials after 15 min.

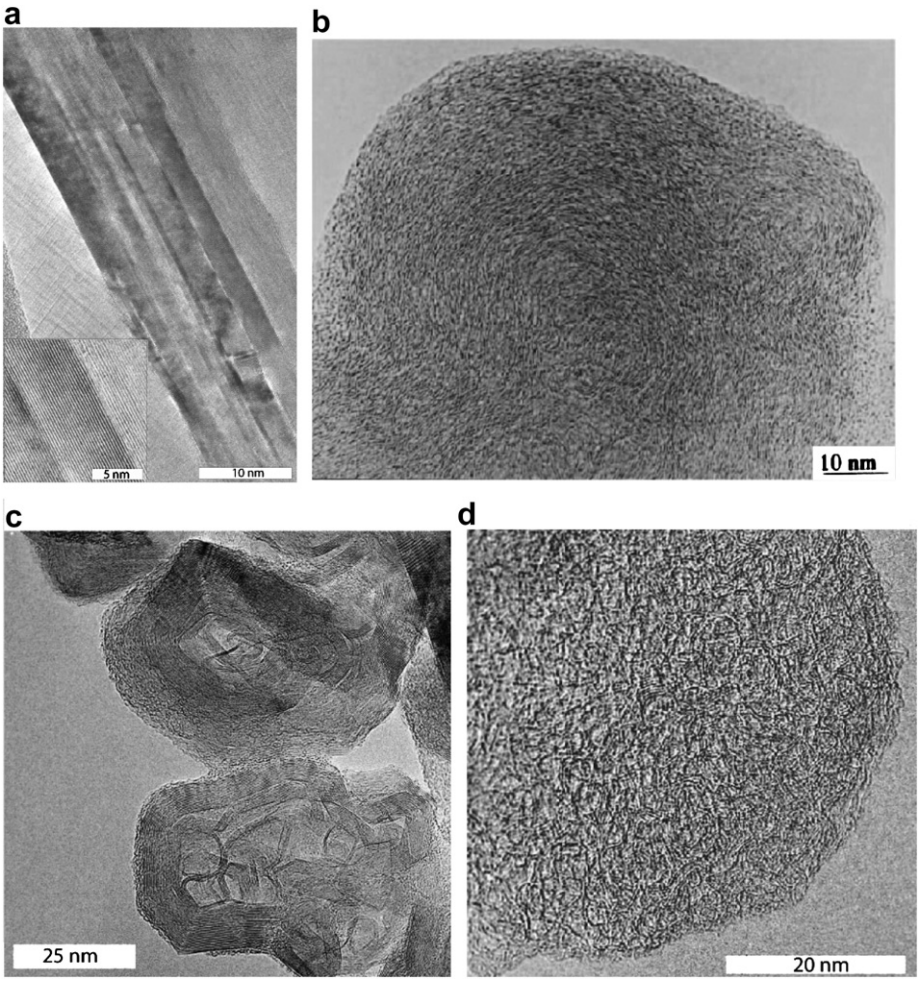

Fig. 3. HRTEM images showing the 002 lattice fringe of the starting materials: polycrystalline graphite (a), carbon black (b), heat treated carbon black (c) and quasi-amorphous soot (d).

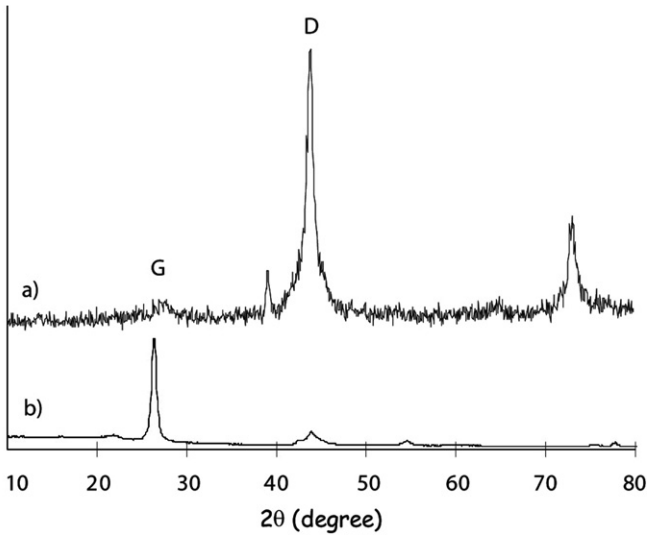

Fig. 4. XRD pattern obtained after 15 min at 15 GPa and 1500 °C: (a) quasi-amorphous soot, (b) carbon black and (c) polycrystalline graphite.

Nevertheless, the transformation rate is higher for starting materials with disordered structures (Fig. 4).

It should be emphasized that PCG and HTCB which have the same initial structural order (as inferred by Raman microspectrometry) but a different microtexture, show no significant difference in their transformation rate (Table 1).

Under the same pressure and temperature conditions (15 GPa and 1500 °C) but after 30 min, CB and QAS have been almost completely transformed into diamond whereas PCG diffraction pattern still shows 002 reflections from remaining graphitic material. Full transformation into diamond is achieved after 60 min for QAS and CB according to XRPD although, optically, the run product is still not fully transparent. Comparatively, the QAS sample is more transparent than the CB one.

After 15 min at 15 GPa and 1700 °C, XRPD shows that CB has fully transformed into diamond, while, again, graphitic 002 reflections are still present in the PCG run product. These samples (CL2SM1, CL2SM3) are still optically black.

It can be concluded at this stage that compared to graphite (PCG), disordered starting-materials (QAS and CB) show higher rates of diamond formation under identical run conditions.

Table 1
Experimental conditions and main results obtained from XRPD and optical observations (pt: partially transparent; t: transparent)

Experiments #	Carbon black (SM3)							Polycrystalline graphite (SM1)					Quasi-amorphous soot (SM4)			Heat treated carbon black (SM5)		HOPG (SM6)
	CL1	CL2	CL3	CL4	CL7	CL8	CL9	CL1	CL2	CL3	CL4	CL10	CL7	CL8	CL9	CL10	CL13	CL13
Temperature (°C)	1500	1700	1900	1500	1500	1500	1500	1500	1700	1900	1500	1500	1500	1500	1500	1500	1700	1700
Pressure (GPa)	15	15	15	15	15	15	15	15	15	15	15	15	15	15	15	15	15	15
Overpressure (GPa)	10.5	10	9.5	10.5	10.5	10.5	10.5	10.5	10	9.5	10.5	10.5	10.5	10.5	10.5	10.5	10	10
Run duration (min)	15	15	15	30	30	60	15	15	15	15	30	15	30	60	15	15	15	15
DG (kJ mol^{-1})	4.8	4.2	3.7	4.8	4.8	4.8	4.8	4.8	4.2	3.7	4.8	4.8	4.8	4.8	4.8	4.8	4.2	4.2
Estimated average grain size	5	7	13	11	7	8	6	4	10	8	12	5		14				
002 Interplanar distance in graphite (nm)	0.33		0.32				0.307	0.34	0.31	0.31	0.32	0.34				0.335	0.317	0.317
Residual internal pressure (GPa)	0		1.5	1.9			5	0	2.5	3.4	2.1					0	2	2
Presence of lonsdaleite	No	No	No	No	No	No	No	No	Yes	Yes	Yes	No	No	No	No	No	Yes	Yes
Presence of residual graphitic carbon (XRPD)	Yes	No	Yes	No	No	No	Yes	Yes	Yes	Yes	Yes	Yes	No	No	Yes	Yes	Yes	Yes
Optical appearance	Black	Black	Black	t	pt	pt	Black	Black	Black	Black	Black	Black	pt	pt	Black	Black	Black	Black

In addition to transformation rates, the yield of lonsdaleite, the hexagonal form of diamond [7], is another difference which has been noticed between ordered and disordered starting materials. At temperatures higher than 1500 °C (*i.e.* at 1700 °C and 1900 °C), a large amount of lonsdaleite could be obtained from HOPG (Fig. 5). Whereas a smaller lonsdaleite amount is obtained from HTCB and PCG (shoulder on the left of the 1 1 1 diffraction peak) while the disordered starting materials did not produce any lonsdaleite (see Fig. 5).

Furthermore, from the XRPD data, it has been possible to estimate the size of our synthetic diamonds by using the Scherrer formula. The average crystal size varies from ~5 nm in half-transformed products to ~10 nm in fully transformed ones (Table 1).

In samples with high diamond yield, 0 0 2 distances as small as 0.307 nm can be found for the remaining carbonaceous material (CM) instead of the expected 0.3354 nm for graphite at ambient pressure. It can then be assumed that these short reticular distances are related to residual stress sustained by the polycrystalline diamond matrix. From hydrostatic compressibility data of graphite [8], this residual pressure (or equivalent hydrostatic pressure) can be

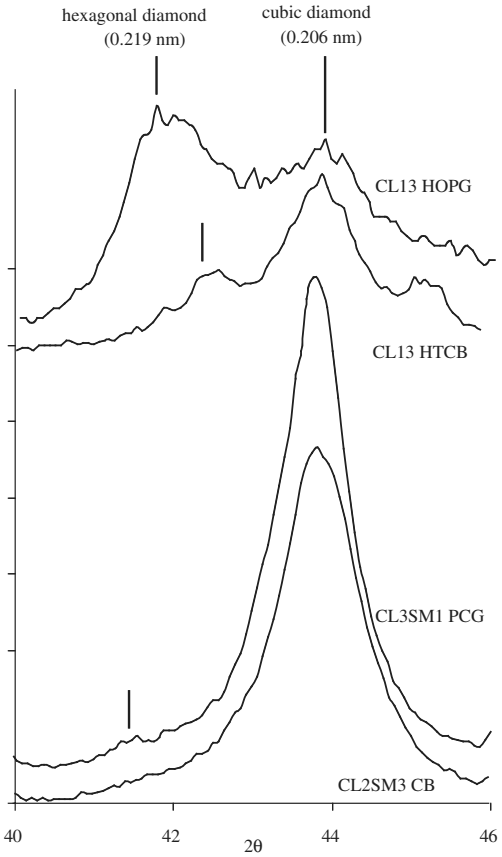

Fig. 5. Detailed X ray diffraction pattern in the vicinity of 1 1 1 cubic diamond reflection (0.206 nm) and 0 0 2 lonsdaleite reflection (0.219 nm). It can be seen that HOPG yielded a high amount of lonsdaleite compared to PCG and HTCB (the shift is due to the different acquisition geometries of the micro-diffraction mode) while no lonsdaleite was found within P25 or QAS (run at 1700 °C).

estimated to ca. 5 GPa. This unreleased stress is also evidenced by Raman micro-spectrometry and HRTEM (see below).

3.3. Raman micro-spectroscopy

The characterization of the run products by Raman micro-spectroscopy is complicated by a strong spatial heterogeneity at the micrometre scale, fluorescence, and a low signal-to-noise ratio. Under the 514.5 nm excitation wavelength, the Raman diffusion cross-section of graphite is 60 times greater than that of diamond. For this reason, the diamond mode cannot be observed in weakly transformed samples. In these samples, however, the R ratio ($R = D1/(G + D1 + D2)$) can be investigated in relation to a possible graphitization state evolution of the starting material. We observe an increase of the relative defect band surface in the transformed products, but only within PCG and HTCB, the graphitized starting materials (Fig. 6).

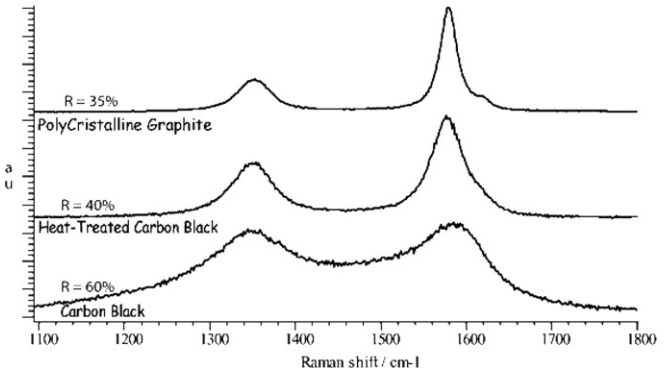

Fig. 6. Raman spectra ($\lambda_i = 514$ nm) of PCG, HTCB and CB held 15 min at 15 GPa and 1500 °C. The D1 relative surface-area has increased only within crystallized products (PCG and HTCB) compared to the starting material.

A nanodiamond spectrum is usually characterized by a broad and faint 1331 cm^{-1} band. The band width can be

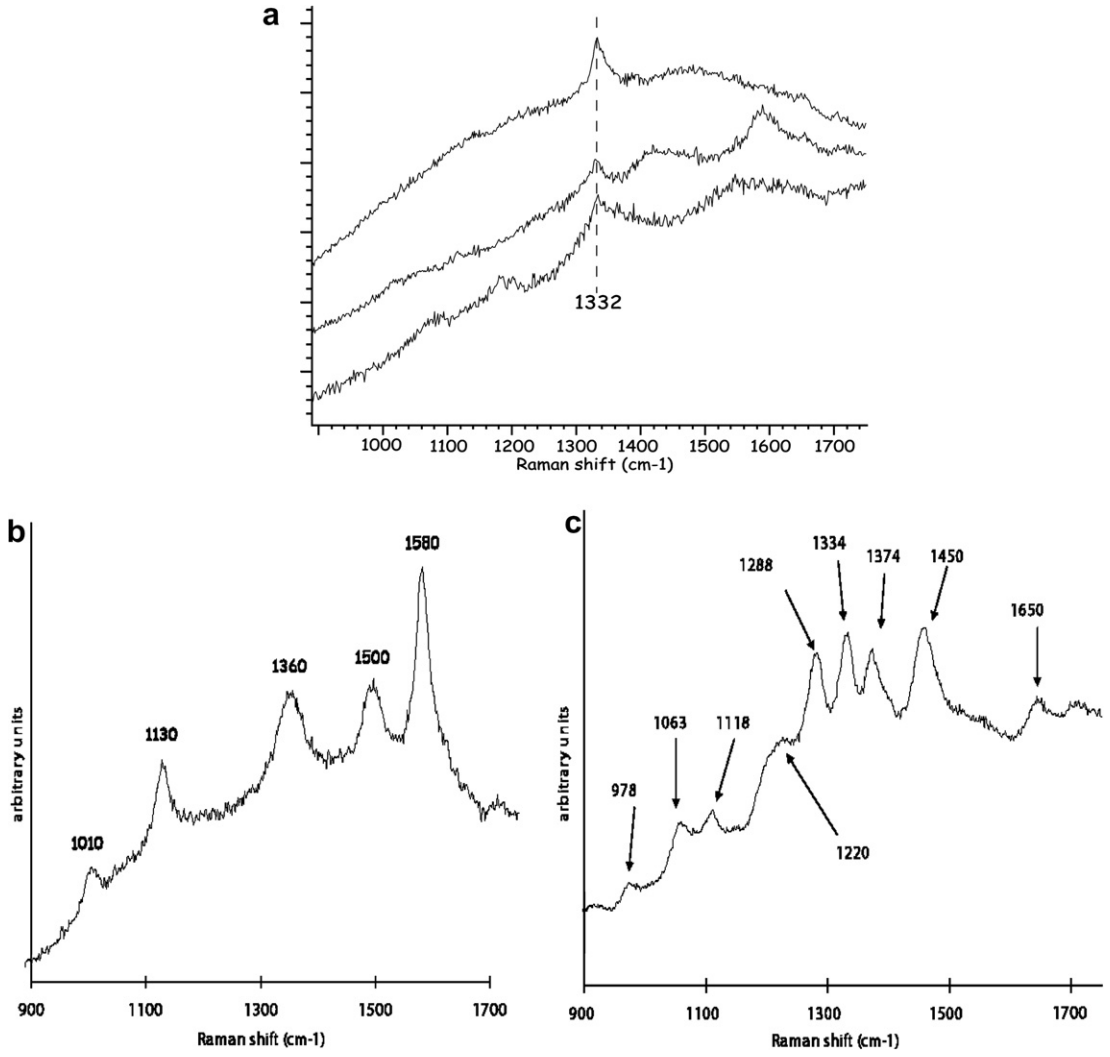

Fig. 7. Typical Raman spectra of highly transformed products showing weak and broad nanodiamond band (~1331 cm^{-1}) together with the sp^2 signature at 1600 cm^{-1} and undetermined bands at 1080, 1180 and 1420 cm^{-1} (CL2SM3) (a); G and D carbon bands together with 1010, 1130 and 1500 cm^{-1} bands (b); upshifted diamond bands (1334 cm^{-1}) together with several and mostly unexplained bands (c).

as large as 50 cm^{-1}, but is generally comprised between 2 and 10 cm^{-1}. The band position is often upshifted by 2–3 cm^{-1} and can even reach 1336 cm^{-1}, what is probably due to residual stress (Fig. 7a).

Furthermore, samples containing mostly diamond display, beside the usual sp^3 diamond mode at 1331 cm^{-1}, a large variety of bands which have not all been reported in the literature (examples are given Fig. 7b and c). The 1080 cm^{-1}, 1200 cm^{-1}, 1350 cm^{-1}, 1500 cm^{-1} and 1580 cm^{-1} bands are classical fundamental and defect modes of graphitic phases [9]. The attribution of the 1150 cm^{-1} and 1400 cm^{-1} Raman bands, also encountered in this study (CL2SM3, CL2SM1), is a matter of debate. It is still unclear whether these bands are related to C–H bonds on the nanodiamond surface [10,11] or to sp^3 nucleus [12], while the 580 cm^{-1} (CL2SM3) and 1280 cm^{-1} bands (CL3SM1, very small amount of lonsdaleite detected in this sample) have been attributed to domain size effect and to the presence of hexagonal diamond, respectively [13,14].

In the optically transparent part of the samples (CL4SM3, CL7SM3, CL7SM4, CL8SM3, CL8SM4, CL9SM4, Table 1), a single band in the 1450–1500 cm^{-1} range is detected using the 514.5 nm incident radiation, but surprisingly no diamond band is visible at 1331 cm^{-1} because of a strong background fluorescence.

For this reason, we tested two other incident wavelengths (UV and IR, respectively). The broad band centred around 1450–1500 cm^{-1} is confirmed by using a 735 nm laser, and seems to result from the contribution of at least three bands around 1250 cm^{-1}, 1350 cm^{-1} and 1450 cm^{-1} (Fig. 8). Due to the higher sp^3 cross section under UV excitation (244 cm^{-1}), the diamond mode at 1331 cm^{-1} is enhanced. In addition, a very broad and faint band which remains at around 1600 cm^{-1}, demonstrates the presence of sp^2 bonded atoms in the transparent diamond samples.

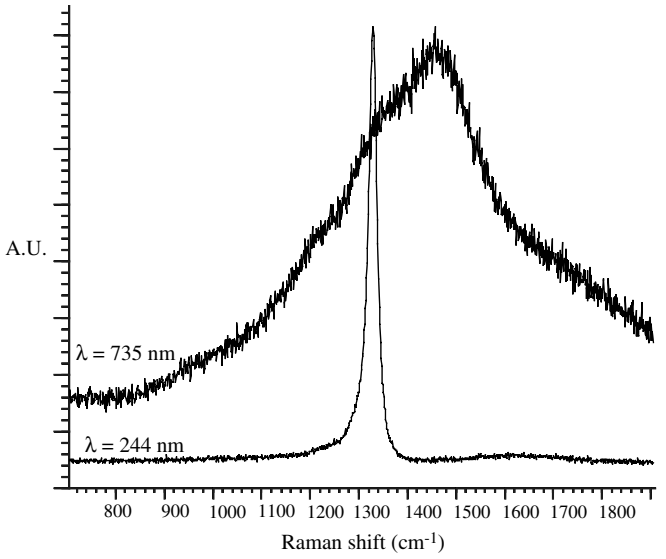

Fig. 8. Raman spectra obtained on transparent diamond samples using two different incident wavelengths: 244 and 735 nm. The diamond mode at 1331 cm^{-1} and the sp^2 contribution, centred around 1450 cm^{-1}, are respectively enhanced. (CL6SM3); (CL1SM1) (c) Delamination of graphite with subsequent decrease of its structural order (CL1SM1). (d) Amorphous carbon coexisting with residual polyhedral heat-treated carbon-black (CL10SM5).

3.4. High resolution transmission electron microscopy

HRTEM confirms the nanometre size (~10 nm) of the diamond crystals, which, according to the images, ranges from about 1 nm to 50 nm.

In order to investigate the transition mechanisms, mutual crystallographic orientation between graphitic phases and diamond can be investigated by imaging the 1 1 1 lattice fringe of diamond (0.206 nm) and the 0 0 2 fringes of the graphitic phases ($\geqslant$0.3354 nm) which correspond to two dense atomic planes of these crystalline carbon phases, respectively.

Two main features of the PCG transformation under pressure and temperature are shown by HRTEM: (1) formation of nanodiamonds in close crystallographic relation with graphite (Fig. 9a and b) and (2) delamination of graphite into strongly disordered carbon (Fig. 9c). It is not excluded, however, that strongly disordered carbon would be the back-transformed product of an unquenchable high-pressure form. Nevertheless, *in situ* XRD measurements on different precursors [8,2,15] have already shown that strong graphite disorganization occurs under pressure and temperature.

Fig. 9a shows 1 1 1 diamond fringes running parallel to the 0 0 2 graphitic ones. This type of observation is consistent with a transition mechanism involving minimum atomic diffusion since the orientation of dense atomic planes remains unchanged through the phase change. Furthermore, Fig. 9a shows that graphitic planes can be strongly deformed at the diamond–graphite interface. On Fig. 9b, deformed graphite 0 0 2 fringes are cross-cut by diamond planes (~70° between them, clearly distinguishable of the 1 0 0 graphite planes ($d_{100} = 0.213$ nm) making a 90° angle with the 0 0 2 ones). This indicates that nucleation occurs within graphite particles and not especially from their surface as it could be suggested by Fig. 9a.

The quasi-amorphous soot (QAS) is a homogenous starting material but with a lower structural order and a lower density. The dense atomic planes of the nanometre-size diamonds formed from the QAS cannot be inherited from the starting material. It could therefore be envisaged that QAS held in the diamond field will encounter graphitization (densification) prior to the diamond nucleation. In sample CL8SM4, held at 1500 °C (15 GPa) for 1 h, the starting soot is not fully transformed into diamond (Table 1). The structure of the remaining soot-material in the vicinity of a diamond crystal can be seen in Fig. 10 (upper right hand side). It appears that no significant graphitization has occurred. The lattice fringe remains short (~1 nm), curved, and still randomly oriented. Accurate

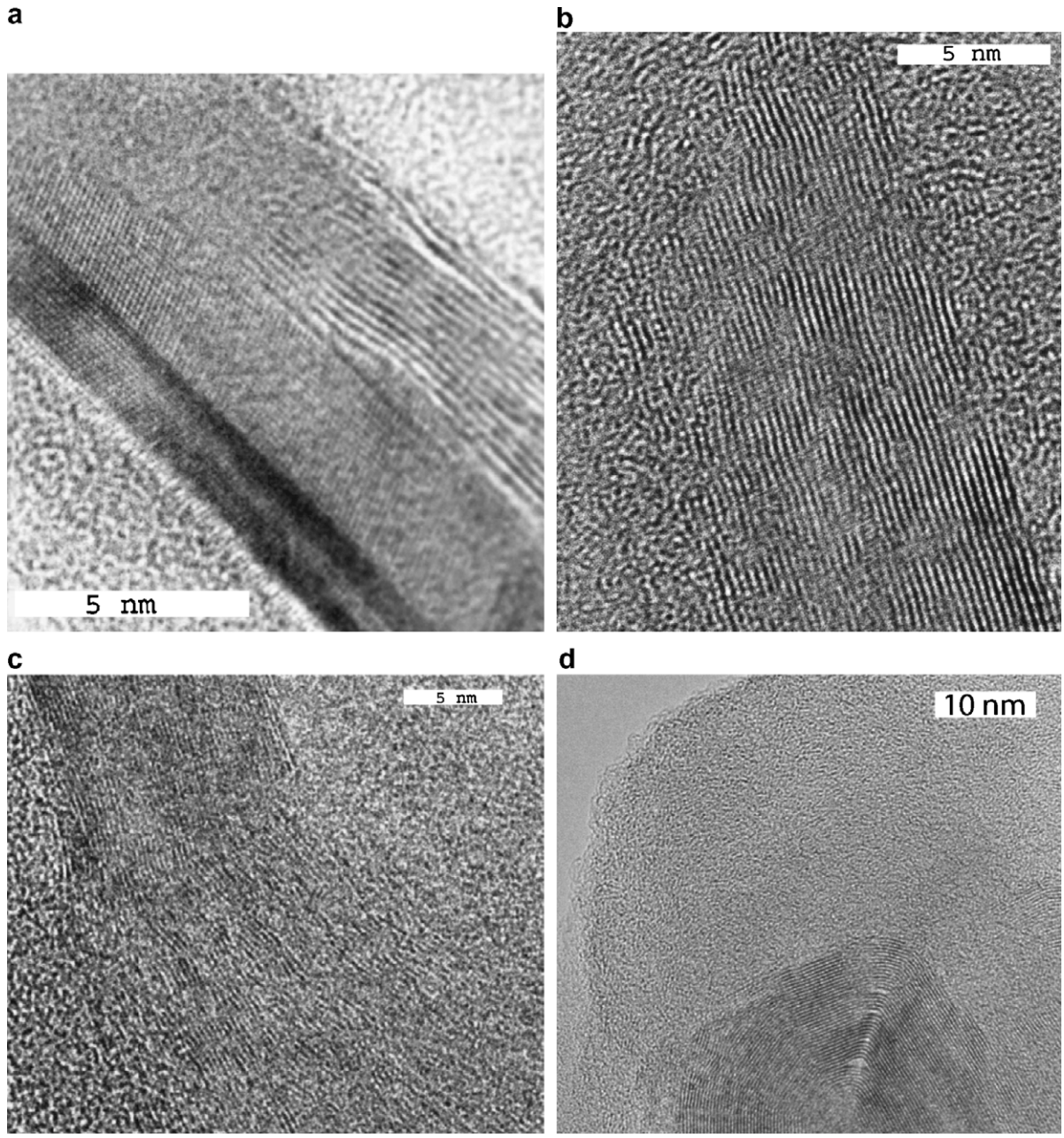

Fig. 9. HRTEM images showing microtextural relation between graphite and diamond. (a) Parallelism between PCG and twinned diamond dense planes (002 and 111, respectively, CL1SM1). (b) 111 diamond planes within wrinkled graphite (CL1SM1). (c) Delamination of graphite with subsequent decrease of its structural order (CL1SM1). (d) Amorphous carbon coexisting with residual polyhedral heat treated carbon black (CL10SM5).

observations of images obtained by focal series, indicates that such fringes cannot be attributed, neither to the effect of the transfer function on crystalline areas out of the Bragg angle, nor to a *stricto sensus* amorphous carbon. This confirms the existence of remnant strongly disordered carbons.

As far as structural order is concerned, carbon black (CB) is intermediate between PCG and QAS. It is a heterogeneous material, and diamond can either nucleate at the rim of the CB which is formed of small polyaromatic layers (1 nm), or within its highly disordered core.

As shown in Fig. 11a (CL1SM3, 1500 °C, 15 min), the concentric shape of the CB particles is preserved and diamond preferentially nucleates in their centre. However, diamond orientation is related to that of the polyaromatic layer. Actually, 111 diamond planes are found to be parallel to the 002 planes of CB contours (Fig. 11b). In this sample, structural improvement starts at the rim of each CB particle. The stacking and the extension of the 002 planes are a slightly higher than those of the starting material. However, this evolution is weak and cannot be detected by Raman micro-spectroscopy (see above).

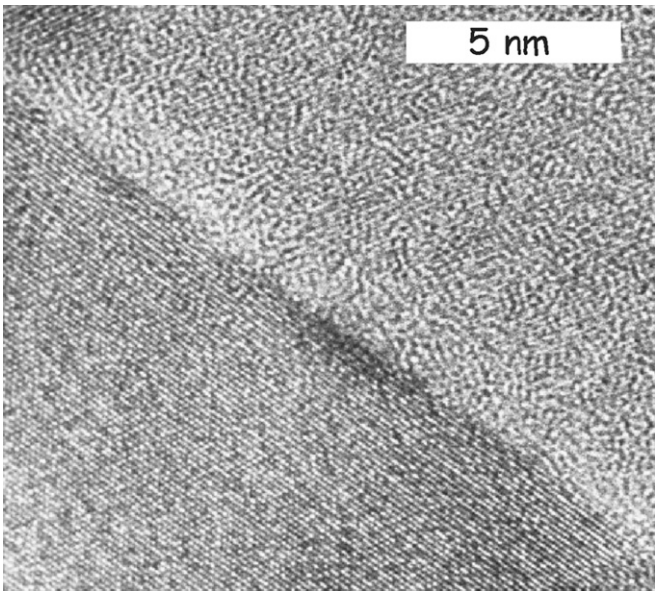

Fig. 10. HRTEM image (CL8SM4) showing a diamond crystal with its 1 1 1 fringes (left-hand side) and the residual 0 0 2 fringes of the soot (right-hand side).

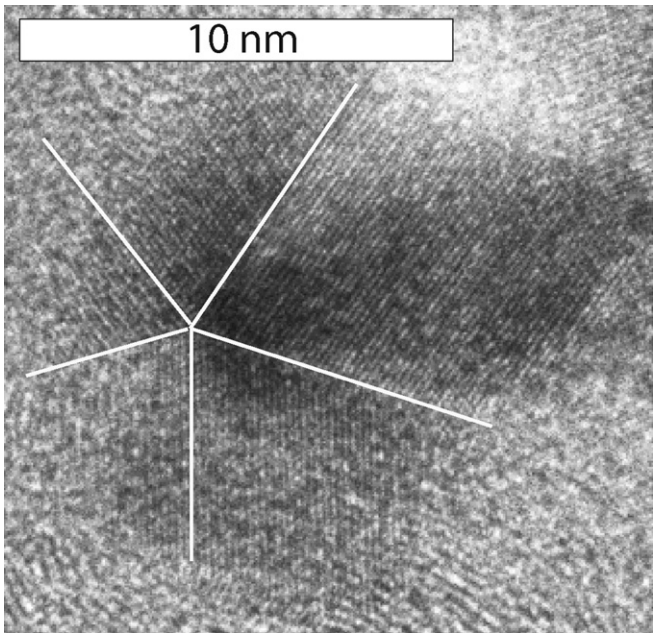

Fig. 12. HRTEM image (CL9SM3) showing a star twin (highlighted in white) in the carbon black heated at 1500 °C (15 GPa) for 30 min.

At 1500 °C, HTCB and PCG yielded comparable diamond amounts. Diamond seems to nucleate in the middle of the HTCB particles. Similarly to PCG, the organization degree has been reduced in the course of the experiment as shown by the increase of the Raman microspectroscopy *R*-ratio (40%). This Raman feature is consistent with amorphous carbon and onions disruption observed by HRTEM (Fig. 9d).

3.5. Diamond twins and residual stress

In addition to the crystallographic relationship between starting materials and transformation products, HRTEM allows to characterize twinning which appears to be abundant in the diamond obtained in this study. In cubic diamond, twinning along the 1 1 1 planes is common and lies on surface-defects as stacking faults or reverse stacking sequence.

Simple (Fig. 9a) and multiple (*i.e.* more than two entities, Figs. 11b and 12) twins are present. They are mostly non linear twins (Fig. 11b and 12). A multiple twin is linear when twin boundaries are parallel and terminate at the crystal surface. It is non-linear when the twin boundaries are not parallel and terminate either at the crystal surface or at their intersection, or both. For example, non linear star-twins (Fig. 12, CL9SM3), previously imaged by Daulton et al., [16] on meteoritic and CVD nanodiamonds are frequently observed.

Finally we have analyzed the HRTEM images with the software developed by Rouzaud and Clinard [17] to evalu-

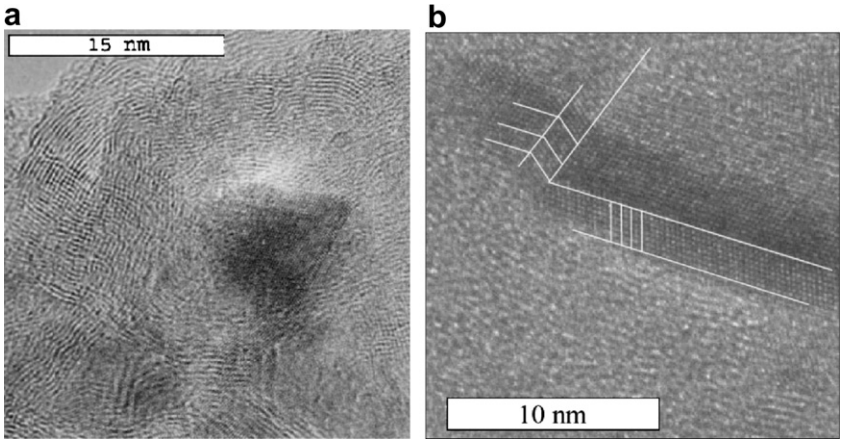

Fig. 11. HRTEM images (CL1SM3) of a diamond grain located in the middle of a remaining CB particle: (a) detailed relation between the diamond grain, its boundary twin and the 0 0 2 fringes of the carbon black. Parallelism between their respective dense planes is observed. (b) Close-up image of the boundary. At the rim of the diamond crystal, linear twins can be seen (highlighted in white).

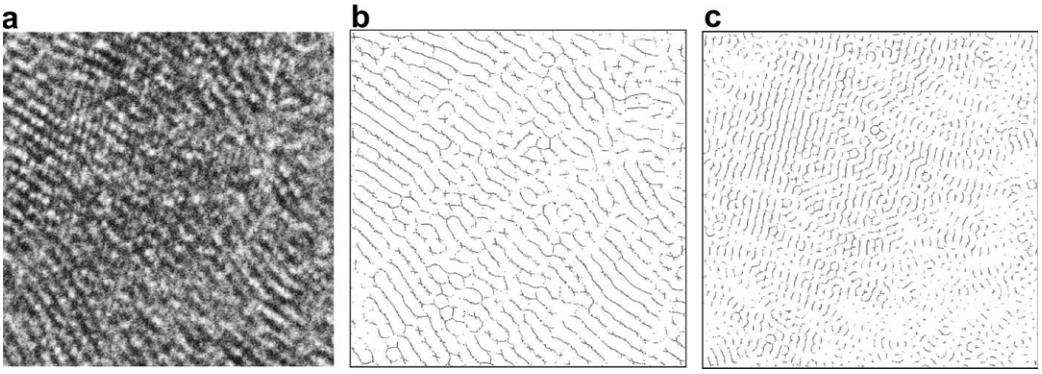

Fig. 13. (a) HRTEM raw image of the carbon black heated at 1500 °C (15 GPa) for 30 min, (b) analyzed 0 0 2 graphitic fringes of the same zone after skelettonization (as-calculated distance between the fringes is about 0.32 nm, *i.e.* smaller than the usual graphite in standard conditions (0.3354 nm)); and analyzed 1 1 1 diamond fringes (as-calculated distance: 0.205 nm).

ate 0 0 2 distances in the graphitic phases coexisting with diamond. Reticular distances between 0.320 and 0.330 nm are obtained for the CB (CLSM3, 1500 °C, 15 GPa, 30 min, Fig. 13). This is slightly higher than the mean value of 0.307 nm indicated by the XRPD data and which corresponds to a residual pressure of ~5 GPa on the graphitic portion. Nevertheless, the XRPD pattern was collected directly on the sample recovered after the experiment without grinding (micro-focus diffraction). By contrast, FIB preparation may favour partial elastic stress relaxation and consequently lead to a noticeable increase of the d_{002} spacing.

4. Discussion

4.1. Thermodynamic

The different starting materials were run at around 10 GPa above the graphite–diamond boundary in the diamond field [18]. Under this overpressure, nanodiamonds have been found to form from a large variety of carbons for temperatures above 1573 K (see [18] for a review). Based on the volume variation (isothermal) of the graphite–diamond transition, it can be calculated that a 10 GPa overpressure corresponds to a driving energy of transformation (ΔG)[1] of *ca.* −5 kJ mol^{-1}. Owing to the low density of the CB and the QAS, this driving energy value is expected to be even higher for these materials.

Whatever the precursor and the temperature (in the 1500–1900 °C range), nucleation is always the dominant mechanism; growth is limited as shown by the diamond crystal size, typically of 5–20 nm in average (Table 1). Higher temperatures of 2700 °C, at least, are needed to observe significant growth of the diamond crystals [19,20].

Whatever the starting material, diamond nucleation has been achieved under the conditions of our experiments ($T \geqslant 1500$ °C). In other words, nucleation energy barrier for diamond has been overcome for all starting materials. Diamond formation is dominated by nucleation in our experiments. Nevertheless, a slight increase of the crystal size with increasing transformation rates indicates that, to some extend, growth also took place.

For disordered precursors, the transformation into diamond is usually completed within less than 1 h at 1500 °C. Abundant twinning can also be seen as another indication for fast nucleation and growth. The interface at a twin boundary represents one of the lowest-energy lattice defects, and twin microstructures may have a higher formation rate than untwined crystals [16].

4.2. Transformation mechanisms

HRTEM shows that the QAS is not subjected to graphitization prior or during diamond nucleation (Fig. 10). No direct structural relationship is observed between the nanometre sized graphene layers of the soot and the 5–20 nm large diamond-grains. Nucleation is therefore likely to initiate at structural defects between short polyaromatic structures and probably from sp^3 bonds placed at their boundaries rather than within the graphene layers.

The clear absence of significant graphitization to promote diamond formation contrasts with previous studies (*e.g.* [21]) where graphitization of the precursor was claimed to be a requisite for diamond formation.

The situation is very different for PCG which displays a triperiodic structure at the sub-micrometre scale. HRTEM shows that dense atomic planes (1 1 1) of diamond run parallel to those (0 0 2) of remaining PCG. As expected, diamond crystallization, which is a diffusion limited process, is strongly influenced by the pre-existing PCG atomic arrangement. Direct conversion of graphite to diamond has been subjected to numerous studies [8,22,19]. Several transformation routes have been defined, which involve minimum diffusion distances. Theses routes are mostly based on re-stacking and wrinkling of graphite basal planes (see [21] for a review). Crystallographic relationships between graphite and diamond structures suggest that 2 H graphite re-stack into '1H' graphite (AA stacking of large graphene layers) in order to produce 2H diamond

[1] Value calculated from the following equation: $\Delta G = \int_{P_{eq}}^{P_{exp}} \Delta V T \mathrm{d}P$ using thermodynamical parameter (compressibility) from [23].

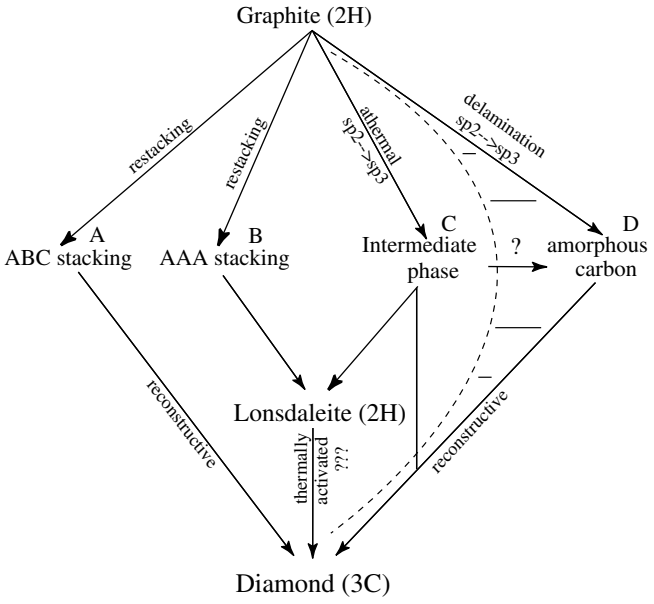

Fig. 14. Tentative sketch summarising possible transformation paths leading from graphite or amorphous carbon to lonsdaleite or diamond based on literature data (paths on the left-hand side) and on results obtained in this study (paths on the right-hand side). The dashed line indicates that amorphisation during delamination may be partial. Nevertheless, it is not excluded that delamination could result from unquenchable intermediate phases (as AA stacking or the so called intermediate phase).

(*i.e.* lonsdaleite, ABAB stacking, Fig. 14, path B). Similarly, re-stacking into 3R graphite (rhombohedral graphite, ABC stacking) is required to yield 3C diamond (or cubic diamond) according to a minimum diffusion process (Fig. 14, Path A). Other routes (kinetically less favourable) involving re-stacking of diamond, from 2H to 3C, can also be proposed. In all these cases, the 0 0 2 graphite planes will correspond to 1 1 1 planes in diamond, in good agreement with the observations made here.

As far as high-pressure experiments are concerned, it has been recognized for long that cold compression of graphite above 15 GPa can induce a phase transition towards a low resistivity form [24,7]. The structure of this high-pressure form of carbon is related to that of 2H diamond but, unlike hexagonal diamond, it cannot be quenched and graphite is recovered instead [8]. Recently, Mao et al. [22], were able to show that cold-compression of graphite above around 15 GPa, leads to an unquenchable intermediate phase (between graphite and hexagonal diamond) where one half of the sp^2-hybridized carbons are shifted out the polyaromatic layers and change to a sp^3 hybridization while the XRD pattern still indicates the presence of graphite-like structure.

In our experiments, this intermediate structure may have been (partly) attained before the PCG sample is heated, in the course of the compression stage (see Section 2). Heating of the sample could then promote the transformation of this intermediate phase to hexagonal diamond by shifting the remaining sp^2 carbon (Fig. 14, Path C). The transformation from hexagonal to cubic diamond corresponds to a modification of the stacking sequence which is thermally activated [8].

It must be noted that the PCG sample that we used here does not correspond to highly crystalline graphite compared to HOPG. Structural defects in PGC account for an R ratio of 15%. We propose that rather than being erased by a graphitization process, these defects serve as diamond nucleation sites. They are mostly located at the crystallite surface. Some HRTEM images do suggest that the replacement of PCG grains by diamond proceeds from their surface. Delamination of the graphitic planes shows that graphitization is not favoured in the pressure and temperature range investigated here. An alternative is that restacking of PCG into '1H' graphite has occurred but this form could not be quenched.

HRTEM shows crystallites with highly wrinkled graphitic layers (Fig. 9c). This delamination feature can ultimately lead to an amorphous-like carbon (Fig. 9d). In agreement with an increase of the defects amount, Raman spectroscopy shows that the R ratio increases from 15% to 35% (CL1SM1 and CL10SM1). This well agrees with Onodera et al. [2] who already mentioned delamination of graphite under high pressure (10 GPa) prior to diamond nucleation.

Furthermore, XRPD on extensively transformed PCG always indicates that lonsdaleite is present, but in small amount (Fig. 5).

On these bases, two end-member transformation schemes can be proposed for the PCG samples, which are likely to operate simultaneously:

(i) In a process that would minimize atomic diffusion, PCG could transform to cubic diamond through a hexagonal diamond stage (Fig. 14, Path B or C). This would explain why hexagonal diamond is partly recovered in these PCG samples, and why cubic diamond and PCG share crystallographic relationships.
(ii) Original defects in PCG and those resulting from the delamination of the graphitic structure could control the diamond nucleation and growth (Fig. 14, Path D). This transformation scheme does not involve an intermediate hexagonal diamond stage. Therefore it would explain why the hexagonal diamond yield is much lower in PCG than for a defect-free graphite (HOPG) run under the same P–T conditions.

Experiments using HOPG as starting material brings an additional insight into diamond formation mechanisms. Compared to HTCB which was run in the same experiment (at 1700 °C, 15 GPa, 15 min), the hexagonal diamond yield is incredibly larger with HOPG. HTCB is a graphite-like material made of partially graphitized hollow polyhedra which displays the same amount of defects as PCG (Raman micro-spectrometry data). Nucleation and diamond growth are likely to be partly controlled by these defects in HTCB. This formation process which is mostly recon-

structive favours cubic diamond (Fig. 14, Path C or D) what explains the very low lonsdaleite yield when using HTCB. In the case of HOPG, the lack of defects at the beginning of the experiments favours hexagonal diamond according to the re-stacking transformation route as described in Fig. 14, Path B or C. Simultaneously, delamination of HOPG may create defects which will rather lead to cubic diamond nucleation and growth (Path D).

Finally, carbon black (CB) appears as a key starting-material to understand the diamond formation mechanisms since it has a heterogeneous structure (see Section 3.1) with a partly amorphous inner-part and a graphitic rim. The main observation is the preferred nucleation of diamond in the middle of the spherical particles while the rims have undergone a weak structural improvement. This supports the idea that sp^3 hybridized carbons, the concentration of which is the highest in the inner CB particle shell, favour diamond nucleation. In the raw CB, the extension of the polyaromatic layers (about 1 nm) and their local rough parallelism are sufficient to impose their orientation to the nano-diamonds as shown by the parallelism between 1 1 1 diamond and 0 0 2 graphitic fringes.

It must be noted that no lonsdaleite is observed in these samples. This is consistent with the view of lonsdaleite as an intermediate product of cubic diamond formation from highly graphitized starting materials (according to Path B or C). The Raman *R* ratio in the starting material is already high (~60%), it does not evolve during the transformation.

Local anisotropic stress has been proposed as a controlling parameter over the graphitization process [25]. This was the incentive to compare two products with the same Raman *R*-ratio, one with large grains made of randomly oriented graphite crystallites (PCG) and the other with nano-particles characterized by a polyhedral microtexture (HTCB). XRD has demonstrated that for experiments at 1500 and 1700 °C (15 GPa) for 15 min about the same volume fraction had been transformed. It has also been shown that the relative orientation of the graphite grain regarding to that of the maximum stress direction can lead to different microtextures in polycrystalline (rounded grains vs lamellar structure) aggregates through different mechanisms (diffusive vs martensitic, respectively); [19].

Diamond formation processes and kinetics seem to depend on the structural state, as quantified by the *R*-ratio, rather than on the microtexture through possible local stress effect. The hardness of the polycrystalline diamond aggregates obtained in this study allows sustaining high internal pressures as evidenced by compressed graphite. The shift of the 0 0 2 XRPD peak indicates a residual pressure, in all the extensively transformed samples, of up to 5 GPa ($d_{002} = 0.307$ nm) according to room-temperature graphite compressibility [8]. It is also possible to observe smaller interfringes distances by HRTEM on FIB prepared samples. This shows that, contrary to grinding, this thinning technique can preserve internal stresses (at least partly).

In relation to a rapid diamond formation, abundant twinning is observed. Based on microstructural differences observed by HRTEM between synthetic and meteoritic nanodiamonds, Daulton et al., [16], have proposed that the ratio between single and twinned crystals depends on the transformation rate. They also show that the ratio between linear twins, with parallel domain boundary, and non-linear twins with non-parallel domain boundary depends on the hydrostaticity of the formation medium. In our study, we mostly observed non-linear twins what is consistent with the use of a quasi-hydrostatic pressure medium (sodium chloride).

Once transformation mechanisms have been addressed, transformation kinetics can be dealt with. Quantification of transformation rates in our experiments is difficult using XRPD. Actually, an accurate proxy is the optical aspect of the product which varies from black to transparent, even in samples in which remaining traces of starting material cannot be detected with XRPD. In these latter samples, it can be argued that the corresponding remain of starting material requires a higher thermal energy to convert into diamond. This would be consistent with the scheme of various transformation mechanisms in a single sample.

In light of our experimental data, it appears that the less graphitized the starting material, the more transparent the diamond product (at a given temperature). This strongly suggests that route D in Fig. 14 is that of the lowest energy. This is probably due to the presence of defects (crystal surface termination, sp^3 hybridized bonds) and linked to the higher molar volume (low density) of those materials. The other transformation routes involving re-stacking of graphitic layers (or diamond ones) are less favourable under the experimental conditions investigated here. For graphitized starting material, a delamination stage allows the development of the partial disorder required to take route D, kinetically, more favourable.

5. Conclusion

Nanodiamond nucleation and growth has been investigated below 2273 K at 15 GPa from carbons covering a wide range of structural organizations. We have shown that graphitization of disordered carbons is not a requisite to the formation of nanodiamonds. On the contrary, it was even necessary for graphite to go through a partial amorphization (loss of long range order) to allow diamond nucleation (and growth). As a consequence, disordered carbons and especially amorphous ones appeared as the starting materials which require the least thermal energy to transform into nanodiamond at 15 GPa.

Acknowledgements

F.B., C.L. and J.N.R. stays in Japan were funded by JSPS and CNRS. Special thanks are due to Bruno Goffé for decisive discussion at the beginning of this project.

Dr. H. Sumiya (Sumitomo) is acknowledged for sharing his knowledge of industrial diamond synthesis. Preliminary experiments were carried out at the LMV (Clermont-Fd, France) on the multi-anvil (INSU Facility) under the guidance of T. Hammouda and N. Bolfan-Casanova.

References

[1] Higashi K, Onodera A. Non-catalytic synthesis of diamond from amorphous carbon at high static pressure. Physica B+C 1986;139–140:813–5.
[2] Onodera A, Irie Y. Graphitization of amorphous carbon at high pressure to 15 GPa. J Appl Phys 1991;69:2611–7.
[3] Tuinstra F, Koenig JL. Raman spectra of graphite. J Chem Phys 1970;53:1123–30.
[4] Beyssac O, Goffe B, Petitet JP, Froigneux E, Moreau M, Rouzaud JN. On the characterization of disordered and heterogeneous carbonaceous materials by Raman spectroscopy. Spectrochim Acta Part A 2003;59:2267–76.
[5] Irifune T, Kurio A, Sakamoto S, Inoue T, Sumiya H. Ultrahard polycrystalline diamond from graphite. Nature 2003;421(6923):599–600.
[6] Oberlin A. High resolution TEM studies of carbonization and graphitization. In: Thrower PA, editor. Chemistry and physics of carbon, vol. 22. New York: Dekker; p. 1–143.
[7] Bundy FP, Kasper JS. Hexagonal diamond – a new form of carbon. J Chem Phys 1967;46(9):3437–46.
[8] Yagi T, Utsumi W. High pressure in situ X-ray-diffraction study of the phase transformation from graphite to hexagonal diamond at room temperature. Phys Rev B 1992;46(10):6031–9.
[9] Kawashima Y, Katagiri G. Fundamentals, overtones and combinations in the Raman spectrum of graphite. Phys Rev B 1995;52(14):10053–9.
[10] Ferrari AC, Robertson J. Origin of the 1150-cm^{-1} Raman mode in nanocrystalline diamond. Phys Rev B 2001;63:121405 R1–4.
[11] Michaelson S, Hoffman A. Hydrogen bonding, content and thermal stability in nano-diamond films. Diamond Relat Mater 2006;15(4–8):486–97.
[12] Schröder RE, Nemanich RJ, Glass JT. Analysis of the composite structures in diamond thin films by Raman spectroscopy. Phys Rev B 1990;41(6):3738–45.
[13] Yoshikawa M, Mori Y, Maegawa M, Katagiri G, Ishida H, Ishitani A. Raman scattering from diamond particles. Appl Phys Lett 1993;62:3114–6.
[14] Gogotsi Y, Kailer A, Nickel KG. Pressure-induced phase transformations in diamond. J Appl Phys 1998;84(3):1299–304.
[15] Brazhkin V, Lyapin AG, Voloshin RN, Popova SV, Klyuev YA, Naletov AM, et al. Mechanism of the formation of a diamond nanocomposite during transformations of C_{60} fullerite at high pressure. JEPT Lett 1999;69(11):869–75.
[16] Daulton TL, Eisenhour DD, Bernatowicz TJ, Lewis RS, Buseck PR. Genesis of presolar diamonds: comparative high resolution transmission electron microscopy study of meteoritic and terrestrial nano-diamonds. Geochim Cosmochim Acta 1996;60(23):4853–72.
[17] Rouzaud JN, Clinard C. Quantitative high resolution transmission electron microscopy: a promising tool for carbon materials characterization. Fuel Process Technol 2002;77–78:229–35.
[18] Bundy FP, Bassett WA, Weathers MS, Hemley MJ, Mao HK, Goncharov AF. The pressure–temperature phase and transformation diagram for carbon. Updated through 1994. Carbon 1996;34:141–53.
[19] Sumiya H, Irifune T, Kurio A, Sakamoto S, Inoue T. Microstructure features of polycrystalline diamond synthesized directly from graphite under static high pressure. J Mater Sci 2004;39:445–50.
[20] Irifune T, Kurio A, Sakamoto S, Inoue T, Sumiya H, Funakoshi K. Formation of pure crystalline diamond by direct conversion of graphite at high pressure and temperature. Phys Earth Planet Interiors 2004;143–144:593–600.
[21] Sungh J. Graphite to diamond transition under high pressure: a kinetics approach. J Mater Sci 2000;35:6041–54.
[22] Mao LW, Mao H, Eng JP, Trainor T, Newville M, Kao C, et al. Bonding changes in compressed superhard graphite. Science 2003;302:425–7.
[23] Le Godec Y, Martinez-Garcia D, Solozhenko VL, Mezouar M, Syfosse G, Besson JM. Compression and thermal expansion of rhombohedral boron nitride at high pressure and temperature. J Phys Chem Solids 2000;61:1935–8.
[24] Aust RB, Drickamer HG. Carbon: a new crystalline phase. Science 1963;140:817–9.
[25] Bustin RM, Rouzaud JN, Ross JV. Natural graphitization of anthracite: experimental considerations. Carbon 1995;33(5):679–91.